Effect of random walk phase noise on MIMO measurements

Almers, Peter; Wyne, Shurjeel; Tufvesson, Fredrik; Molisch, Andreas

Published in:
[Host publication title missing]

DOI:
10.1109/VETECS.2005.1543266

2005

Effect of Random Walk Phase Noise on MIMO Measurements

Peter Almers[1,2], Shurjeel Wyne[1], Fredrik Tufvesson[1] and Andreas F. Molisch[1,3]
[1] Dept. of Electroscience, Lund University, Box 118, SE-221 00 Lund, Sweden.
[2] TeliaSonera AB, Box 94, SE-201 20 Malmö, Sweden.
[3] Mitsubishi Electric Research Labs, Cambridge, MA 02139, USA.
Email: {Peter.Almers, Shurjeel.Wyne, Fredrik.Tufvesson, Andreas.Molisch}@es.lth.se

***Abstract*— In this paper we study the influence of phase noise from free-running local oscillators on SAGE signal parameter estimation. Phase noise is here modeled as a random-walk process. We present phase noise estimates from our LUND RUSK MIMO channel sounder, and draw conclusions on requirements on local oscillators' phase noise in terms of the Allan variance. We investigate an error propagation effect in SAGE, and finally, we present random-walk phase noise effect on channel capacity.**

I. Introduction

Multiple-input multiple-output (MIMO) wireless communication systems have multi-element antenna arrays at both the transmitter and the receiver side. It has been shown that they have the potential for large information-theoretic capacities since the system can provide several independent communications channels between transmitter and receiver [1], [2], [3].

Measurements of the spatial radio channel [4] are vital for understanding the MIMO channel and for system design, simulations and performance analysis. The most popular method for obtaining such measurements is by a channel sounder with a switched array, where the elements of an antenna array are connected, one after the other, to a "conventional" channel sounder measuring impulse responses [5]. However, MIMO measurements obtained by either this, or any other, principle suffer from several error sources in addition to thermal additive white Gaussian noise (discussed in [6], [7]), e.g. phase noise (PN) during the measurements and array calibration errors.

PN, i.e. frequency fluctuations of the local oscillators (LOs) in the transmitter and receiver, can be divided into two main categories: (i) when the system is phase-locked (e.g. transmitter and receiver are connected and use the same LO) the resulting PN is low and modeled as a zero mean, stationary, finite-power random process; (ii) when the system is frequency-locked only, often termed free-running, the resulting PN is slowly varying but not limited, and is modeled as a zero-mean non-stationary infinite power Wiener process, e.g., a random-walk process. While phase-locked measurements can be performed in indoor environments, micro- and macrocellular environments imply a large separation between transmitter and receiver, and thus dictate the use of free-running oscillators.

Several authors have investigated the impact of PN on multi-antenna systems. Kivinen et al. [8] investigated the impact of free-running oscillator PN effect on Fourier-based direction of arrival (DOA) estimation for single-input multiple-output (SIMO) systems. A recent contribution, [9], investigates the impact of PN in phase-locked LOs on the capacity of fully correlated rank-one channels as well as full rank channels.

This paper focuses on the impact of PN from free-running oscillators in MIMO systems, investigating its impact on estimated angles, delay, and Doppler of the multipath components (MPCs), as well as its effect on the estimated channel capacity. In contrast to [8], we study the impact of the PN on the MPC parameters obtained by the *high-resolution SAGE algorithm* [10], which has become the de-facto standard for the evaluation of double-directional measurement campaigns. In contrast to [9], we investigate the impact of *free-running oscillators* on the capacity. We also present PN measurement on our RUSK LUND channel sounder and discuss the error propagation effect in the SAGE algorithm.

The remainder of the paper is organized the following way: Sec. II describes the models and theoretical background for both the SAGE algorithm and the channel capacity, as well as measurements of the PN in our channel sounder. Section III presents the simulation results for the impact of PN on the estimated directions of the MPCs and the capacity. A summary and conclusions wrap up this paper.

II. Theory and Models

A. Oscillator PN Model and Allan Variance

Assume that we have a LO generator with an instantaneous output voltage

$$V(t) = V_0 \sin\left(2\pi f_c t + \varphi(t)\right), \tag{1}$$

where V_0 and f_c are the nominal amplitude and carrier frequency, respectively. The time variations of the frequency are incorporates in the phase noise $\varphi(t)$ and the actual (instantaneous) frequency becomes

$$f(t) = f_c + \frac{d}{dt}\frac{\varphi(t)}{2\pi}. \tag{2}$$

The phase noise is the difference between phase of the carrier and the phase of the LO, and the fractional frequency deviation is defined as [11], [12]

$$y(t) = \frac{f(t) - f_c}{f_c} = \frac{d}{dt}\frac{\varphi(t)}{2\pi f_c}. \tag{3}$$

If the system is only frequency locked but not phase locked, the LO is said to be free-running. The instantaneous frequency of a free-running LO is well characterized by a fractional frequency deviation, $y(t)$, modelled as a zero mean white Gaussian random process. Since $\varphi(t)$ is obtained by integrating the frequency deviation $y(t)$, the assumptions on $y(t)$ imply that the phase noise $\varphi(t)$ can be described as a random walk process (continuous-path Brownian motion or Wiener–Lévy process) with zero mean and a variance that increases linearly with time. The time-average of the fractional frequency deviation is

$$\begin{aligned}\bar{y}_k(t) &= \frac{1}{\tau}\int_{t_k}^{t_k+\tau} y(t)\,dt \\ &= \frac{\varphi(t_k+\tau)-\varphi(t_k)}{2\pi f_c \tau},\end{aligned} \tag{4}$$

where τ is the averaging period, here equal to the period between two successive measurements, and $t_{k+1} = t_k + \tau$. Another important quantity for the characterization of oscillators is the Allan variance, which is defined as [11], [12]

$$\sigma_y^2(\tau) = \left\langle \frac{(\bar{y}_{k+1}-\bar{y}_k)^2}{2} \right\rangle, \tag{5}$$

where $\langle\cdot\rangle$ defines the infinite-time average. It can be estimated a finite data set as [11], [12]

$$\begin{aligned}\hat{\sigma}_y^2(\tau) &= \frac{1}{K}\sum_{k=1}^{K}\frac{(\bar{y}_{k+1}-\bar{y}_k)^2}{2} \\ &= \frac{1}{K}\sum_{k=1}^{K}\frac{(\varphi(t_{k+2})-2\varphi(t_{k+1})+\varphi(t_k))^2}{2(2\pi f_c\tau)^2}.\end{aligned} \tag{6}$$

In Fig. 1 (a) we present results from back-to-back measurement of the PN in the RUSK LUND MIMO channel sounder. The measurement was performed with a center frequency of 5.4 GHz and a bandwidth of 240 MHz. For the left subplots, the transmit and receive LO were free-running and the plots show the sum of the PN in the transmitter and receiver. In the right subplots, the same LO was used for the transmitter and receiver. The random walk behavior is evident in the upper left subplot. The two LOs are not measured individually, and other sources of noise are present. For shorter time periods, these noise sources dominate and hide the effect of the time dependent random-walk PN, see e.g. second and third subplot to the left. In the paper we only consider the effect of random-walk PN, the effect of PN might be even more pronounced for other PN models. The Allan variance corresponding to the measurements in Fig.1 for the free-running configuration is shown in Fig. 2. Note that the Allan variance is calculated as the sum of the PN in the transmitter and receiver. The Allan variance of the system (sum of transmitter and receiver PN) at 1 s, $\sigma_y(1\text{s}) \approx 7\cdot 10^{-12}$.

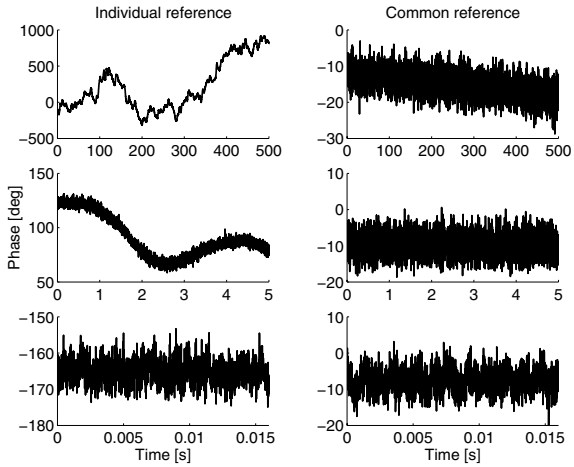

Fig. 1. Phase noise measured from the RUSK LUND MIMO channel sounder, with (a) free running LOs at transmitter and revceiver, and (b) for a common reference.

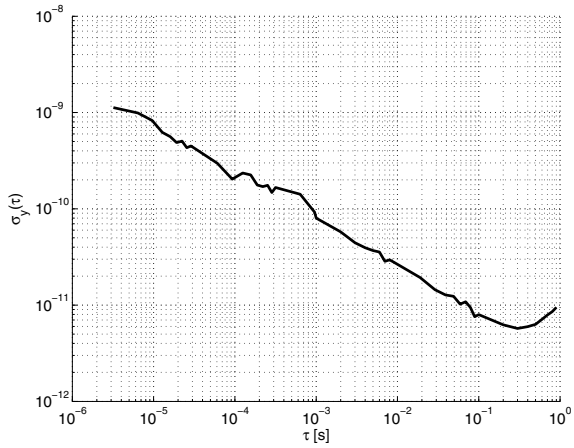

Fig. 2. The $\sigma_y(1\text{s})$ for the RUSK LUND MIMO channel sounder.

B. MIMO Signal Model

In order to obtain a MIMO channel model and extract the parameters of the MPCs, we use the SAGE algorithm [10]. In a first step, the SAGE requires to model the impact of an arbitrary MPC on the received signal $\mathbf{s}$:

$$\mathbf{s}(k,i;\theta_l) = \alpha_l e^{j2\pi(\Delta_t\nu_l i-\Delta_f\tau_l k)}\mathbf{c}_{\text{r}}\left(\phi_l^{(\text{r})}\right)\mathbf{c}_{\text{t}}^T\left(\phi_l^{(\text{t})}\right), \tag{7}$$

where i, is the snapshot number, k is the frequency index, l the index of the considered MPC, and θ_l the set of parameters describing the MPC; this set includes α_l, the complex amplitude, ν_l, the Doppler frequency, τ_l, is the delay and $\phi_l^{(\text{r})}$, $\phi_l^{(\text{r})}$ is the direction of arrival (DOA) and direction of departure (DOD). Furthermore, Δ_t is the time between snapshots, Δ_f is the spacing between measured frequencies, and $\mathbf{c}_{\text{r}}$ and $\mathbf{c}_{\text{t}}$ are the steering vectors at receiver and transmitter, respectively.

For each of the N_{t} transmit elements, we assume that the N_{r} receive elements at the receiver are swept with an element switching time of T_{mux}. Hence, the switching time between transmitter array elements is then $N_{\text{r}}\cdot T_{\text{mux}}$, and the time between two consecutive snapshots is $N_{\text{r}}\cdot N_{\text{t}}\cdot T_{\text{mux}}$. We assume that the random-walk PN affects all frequency sub-channels of the multicarrier spread spectrum test signal equally, due to the short time duration of the test signal. Thus the PN corrupted

signal is modelled as

$$\mathbf{s}_{\text{PN}}(k,i;\theta_l) = \mathbf{s}(k,i;\theta_l) \odot \mathbf{N}_i, \tag{8}$$

where $\odot$ is the Schur product, and

$$\mathbf{N}_i = \begin{bmatrix} e^{j\varphi_{1,i}} & e^{j\varphi_{N_\text{r}+1,i}} & \dots & e^{j\varphi_{(N_\text{r}(N_\text{t}-1)+1),i}} \\ e^{j\varphi_{2,i}} & e^{j\varphi_{N_\text{r}+2,i}} & \dots & e^{j\varphi_{(N_\text{r}(N_\text{t}-1)+2),i}} \\ \vdots & \vdots & \ddots & \vdots \\ e^{j\varphi_{N_\text{r},i}} & e^{j\varphi_{2N_\text{r},i}} & \dots & e^{j\varphi_{N_\text{r}N_\text{t},i}} \end{bmatrix}, \tag{9}$$

where $\varphi_{q,i} = \varphi\left(qT_{\text{mux}} + (i-1)N_\text{r}N_\text{t}T_{\text{snap}}\right)$ is the random-walk phase error $kT_{\text{mux}} + (i-1)N_\text{r}N_\text{t}T_{\text{snap}}$ seconds after calibration.

C. MIMO Channel Model and Capacity

To investigate the PN effect on channel capacity evaluations, the error in estimated capacity depends on the actual channel transfer matrix, $\mathbf{H}$, in the input-output relation

$$\mathbf{r} = \mathbf{H}\mathbf{x} + \mathbf{n}, \tag{10}$$

where $\mathbf{r}$ is the received column vector, $\mathbf{x}$ is the transmit column vector and $\mathbf{n}$ is the additive white Gaussian noise column vector. We focus on the worst-case scenario, that is the one that minimizes the channel capacity. This occurs when the channel transfer matrix has a single eigenmode, i.e., only one nonzero eigenvalue. A channel matrix that satisfies this condition is the keyhole channel [13], [14] defined as

$$\mathbf{H}_{\text{key}} = \mathbf{g}_\text{R}\mathbf{g}_\text{T}^\dagger, \tag{11}$$

where $\mathbf{g}_\text{R}, \mathbf{g}_\text{T}$ are column vectors distributed as $\mathbf{g}_\text{R}, \mathbf{g}_\text{T} \in \mathcal{CN}\left(\mathbf{0}, \sigma^2_{\text{key}}\mathbf{I}\right)$, thus the entries are uncorrelated [13]. The transfer matrix corrupted by PN is then defined as

$$\mathbf{H}_{\text{PN}} = \mathbf{H}_{\text{key}} \odot \mathbf{N}_i. \tag{12}$$

The instantaneous capacity is [2], [3]

$$C = \log_2 \det\left(\mathbf{I}_{\max(N_\text{r},N_\text{t})} + \frac{\gamma}{N_\text{t}}\mathbf{W}_\mathbf{H}\right), \tag{13}$$

where

$$\mathbf{W}_\mathbf{H} = \begin{cases} \mathbf{H}\mathbf{H}^\dagger & \text{for } N_\text{r} \le N_\text{t} \\ \mathbf{H}^\dagger\mathbf{H} & \text{for } N_\text{r} > N_\text{t} \end{cases}. \tag{14}$$

and $\mathbf{I}_{\max(N_\text{r},N_\text{t})}$ is an identity matrix of size $\max(N_\text{r}, N_\text{t}) \times \max(N_\text{r}, N_\text{t})$. The results of the capacity evaluations are presented in the next section.

III. Simulation Results

To analyze the influence of the PN on the MPC parameters as estimated by SAGE, we study two scenarios: (i) a synthetic scenario with a single MPC, and (ii) a realistic scenario with 10 MPCs. The parameters used for the simulations are presented in Table I.

As a criterion of the error, we use the root mean square error (RMSE) for the DOA and DOD, defined as

$$\varepsilon_{\text{RMSE}} = \sqrt{\sum_n |x - \hat{x}_n|^2}, \tag{15}$$

TABLE I

Parameters used for simulations

SAGE parameters	Value
No iterations (for RMSE)	100
No SAGE iterations	40
No snapshots	20
T_{mux}	5 μs
$\phi_1^{(\text{r})}, \phi_1^{(\text{t})}$ (for single MPC)	0

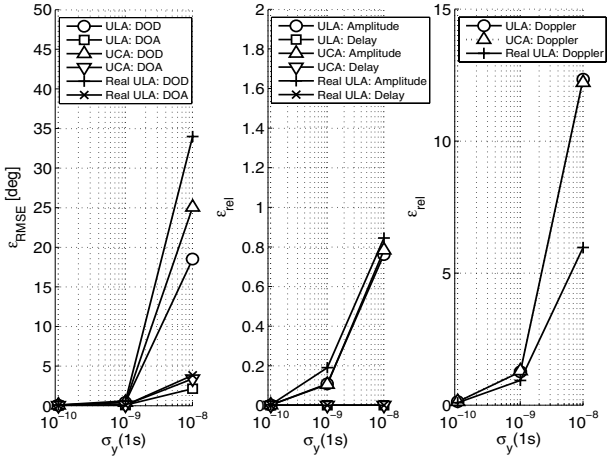

Fig. 3. RMSE versus $\sigma_y(1\text{s})$ for an 8×8 ULA system, an 8×8 UCA system both with uniform element responses, and, finally, RMSE for a real patch ULA antenna. The MPC departure and arrives at broad side of the ULAs.

where n is the iteration number. For delay, amplitude and Doppler frequency the relative error, ε_{rel}, is used as error measure, defined as

$$\varepsilon_{\text{rel}} = \frac{1}{\sum_n 1}\sum_n \frac{|x - \hat{x}_n|}{x}. \tag{16}$$

A. Single MPC

In Fig. 3 the effect of random-walk PN on estimated DOA, DOD, amplitude, delay and Doppler frequency is presented for a single MPC when using a 8×8 systems with: two uniform linear arrays (ULAs), two uniform circular arrays (ULAs) (ULA and UCA, both with ideal uniform antenna patterns) and finally, a 8×8 system with two real patch ULAs (i.e. with directional antenna patterns, see [15] for details).

The DOD is more affected by random-walk PN than the DOA, due to the N_r-times longer element switching time between transmitter elements. The UCA seems to be more sensitive to random-walk PN than the linear arrays. The directivity of the real array element makes the broadside MPC more affected by random-walk PN, however the amplitude error is similar for all configurations and is a result of mismatch between signal model and the actual signal, including PN. The time between samples for Doppler estimation is $(N_\text{r} \cdot N_\text{t} \cdot T_{\text{mux}})$, thus due to the relative long time between sample of the Doppler frequency its estimates are more effected by the time dependent random-walk PN. The ULA and UCA has a worse Doppler frequency estimate than the real ULA.

In Fig. 4 the effect of array size on the DOA and DOD errors is shown, at an Allan variance of $\sigma_y(1\text{s}) = 10^{-8}$. The

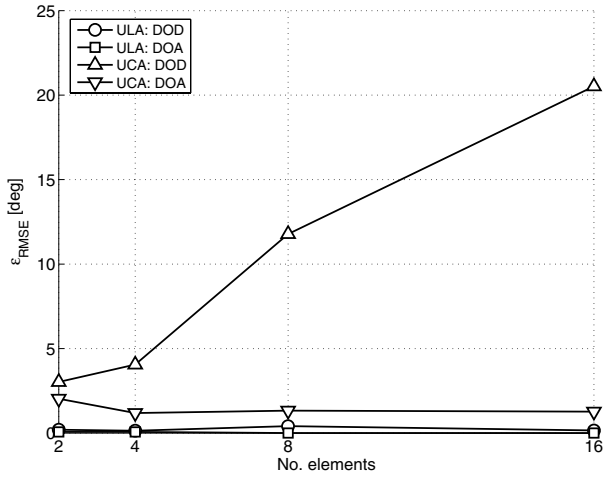

Fig. 4. RMSE versus number of elements of the ULA and UCA arrays at an Allan variance of $\sigma_y\,(1\mathrm{s}) = 10^{-8}$. Each array consists of elements with uniform element responses.

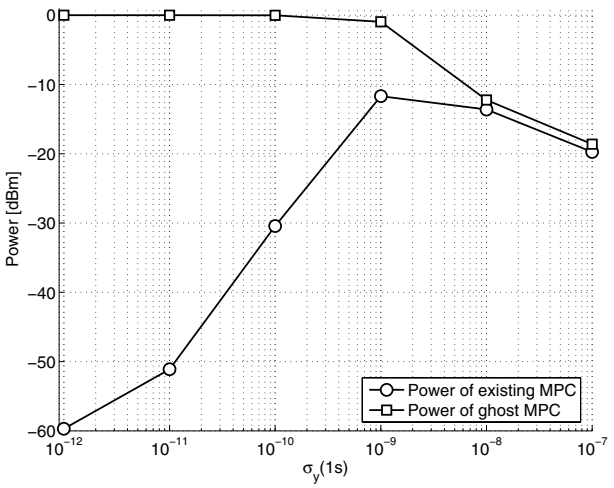

Fig. 5. The power of the existing MPC with a power of 0 dBm and the power of the ghost component as a function of Allan variance.

RMSE of the UCA for DOD increases with the array size, whereas for the DOA the RMSE is almost independent of the array size. For ULA both DOD and DOA appears to be independent of the array size.

B. Error Propagation

When there is a mismatch of the signal model and the measured signal (including PN), the residual of the canceled MPCs might be interpreted by the algorithm as additional MPCs, here denoted ghost components, which physically are non-existing. An estimated ghost component will be used in the next SAGE iteration, hence the error will propagate. The error propagation due to the noise estimation step in the SAGE algorithm [10] is given by

$$y\left(t\right) - \sum_{l'=1}^{L} s\left(t; \hat{\theta}_l'\right), \tag{17}$$

where $y\left(t\right)$ is the measured signal (MIMO channel), $s\left(t; \hat{\theta}_l'\right)$ is the continuous SAGE signal model [10], and $\hat{\theta}_l'$ is the parameter vector for the first estimate ($(\cdot)'$) and the $l-$th MPC.

In Fig. 5 the power of the real MPC and the strongest ghost component is plotted versus the Allan variance. If the ghost component becomes strong enough, it will belong to the set of estimated MPCs. In addition to this, the mismatch of the signal model to the real signal results in a worse correlation and therefore a lower estimated amplitude of the real MPC. Thus, with a measurement dynamic range of 30 dB, the Allan variance has to be less than $\sigma_y\,(1\mathrm{s}) = 10^{-10}$ to suppress the ghost component and avoid the lower correlation gain.

A similar behavior will be present for other signal model mismatches, e.g., when the plane wave assumption does not hold, when the small bandwidth assumption is violated, or due to array calibration errors.

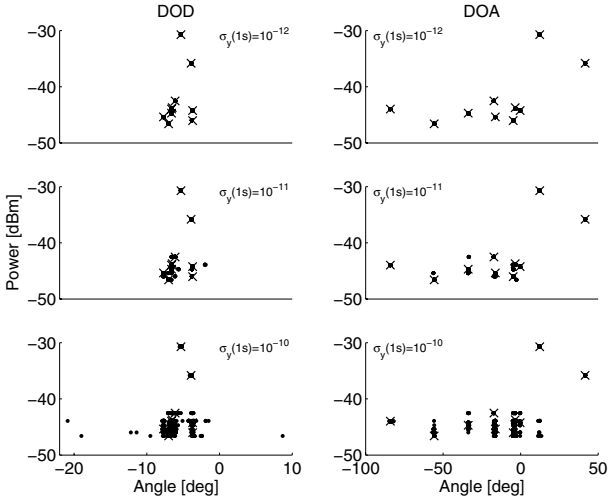

Fig. 6. The DOD, DOA and power estimates (marked with $\cdot$) for 10 MPC generated with the SAGE signal model, for parameters taken from a real LOS measurement scenario (marked with $\times$). The 10 SAGE estimates for each of the 100 channel realizations are marked with $(\cdot)$.

C. Multiple MPCs

Here we evaluate the effect of random-walk PN on estimated SAGE parameters with multiple MPCs, for two scenarios: line-of-sight (LOS) and non-LOS. In order to consider realistic values, we use parameter values of 10 MPCs from a measurement campaign described in [15]. The parameters used for the 10 MPCs are marked with $(\times)$ in Fig. 6 and Fig. 7, for a LOS and a non-LOS scenario, respectively. For each Allan variance, 100 iterations are made and the SAGE estimates are marked with $(\cdot)$. In the figures it can be seen that there are some MPCs that are not detected by SAGE and some MPCs that are ghost components. Here the difference between the strongest and weakest MPCs is less than 20 dB. With a larger dynamic range the effect of error propagation and ghost components will be more pronounced.

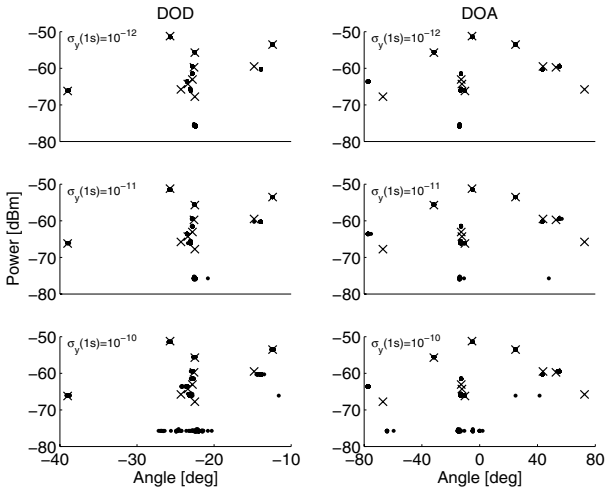

Fig. 7. The DOD, DOA and power estimates (marked with ·) for 10 MPC generated with the SAGE signal model, for parameters taken from a real non-LOS measurement scenario (marked with ×). The 10 SAGE estimates for each of the 100 channel realizations are marked with (·).

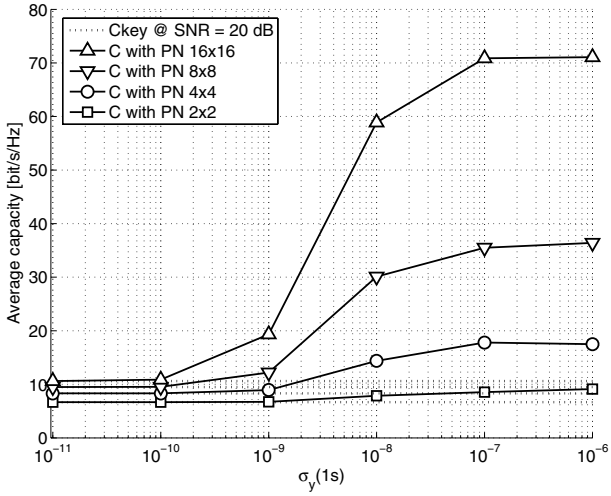

Fig. 8. The average channel capacity versus Allan variance (square root), for different system sizes.

D. PN Effect on Channel Capacity

In Fig. 8 calculations of the average capacity for four different antenna configurations are plotted versus the Allan variance for an evaluation SNR of 20 dB. From the figure it can be concluded that, for this evaluation SNR, the Allan variance of the measurement equipment has to be less than $\sigma_y\,(1\mathrm{s}) < 10^{-10}$ to give capacity values close to the ideal case. Note that due to the properties of the "keyhole" channel, the impact of the PN is maximum. Bad LOs can thus contribute to the problems of measuring "real-life" keyhole channels.

IV. Summary

In this paper we have studied the effect of random-walk PN (in terms of Allan variance of the sum of the PN of two free-running LOs) on the SAGE estimation algorithm. We have study two MIMO scenarios: (i) a synthetic scenario with a single MPC, and (ii) two realistic scenario with 10 MPCs (LOS and NLOS). We discuss an error propagation effect inherent in SAGE and study the resulting ghost components versus the Allan variance. Finally, we present the random-walk PN effect on capacity estimates. From our simulations it seems that the Allan variance of the oscillators should be in the order of $\sigma_y\,(1\mathrm{s}) \leq 10^{-10}$, for an element switching time of $T_{\mathrm{mux}} = 5\mu$s. As a comparison the LUND RUSK MIMO channel sounder has an Allan variance of $\sigma_y\,(1\mathrm{s}) \leq 10^{-11}$. Note that for a longer switching time, the random-walk PN effect will be more pronounced and the requirements on the oscillators become higher. E.g. a doubling of the switch time has the same effect as doubling the Allan variance.

Acknowledgement 1: The authors would like to thank Gunnar Eriksson for his help with the SAGE algorithm. This work was partly funded by an INGVAR grant of the Swedish Foundation for Strategic Research and a grant from Vetenskapsrådet.

References

[1] J. H. Winters, "On the capacity of radio communications systems with diversity in Rayleigh fading environments," *IEEE Journal on Selected Areas in Communications*, vol. 5, pp. 871–878, June 1987.

[2] G. J. Foschini and M. J. Gans, "On limits of wireless communications in fading environments when using multiple antennas," *Wireless Personal Communications*, vol. 6, pp. 311–335, 1998.

[3] I. E. Telatar, "Capacity of multi-antenna Gaussian channels," *European Transactions on Telecommunications*, vol. 10, November–December 1999.

[4] A. F. Molisch, M. Steinbauer, M. Toeltsch, E. Bonek, and R. S. Thoma, "Capacity of MIMO systems based on measured wireless channels," *IEEE Journal on Selected Areas in Communications*, vol. 20, pp. 561–569, April 2002.

[5] R. Thomae, D. Hampicke, A. Richter, G. Sommerkorn, A. Schneider, U. Trautwein, and W. Wirnitzer, "Identification of time-variant directional mobile radio channels," *IEEE Trans. Instrumentation and Measurement*, vol. 49, pp. 357–364, 2000.

[6] P. Kyritsi, R. A. Valenzuela, and D. C. Cox, "Channel and capacity estimation errors," *IEEE Communications Letters*, pp. 517–519, December 2002.

[7] P. Almers, F. Tufvesson, and A. F. Molisch, "Keyhole effects in MIMO wireless channels - measurements and theory," in *Proc. GlobeCom 2003*, vol. 3, (San Francisco, US), pp. 1–5, IEEE, December 2003.

[8] J. Kivinen and P. Vainikainen, "Calibration scheme for syntheizer phase fluctuations in virtual antenna array measurements," *Microwave and optical technology letter*, vol. 26, pp. 183–187, August 2000.

[9] D. S. Baum and H. Boelcskei, "Impact of phase noise on MIMO channel measurement accuracy," in *Proc. IEEE VTC-Fall*, vol. -, (-), pp. –, IEEE, September 2004.

[10] B. H. Fleury, M. Tschudin, R. Heddergott, D. Dahlhaus, and K. I. Pedersen, "Channel parameter estimation in mobile radio environments using the SAGE algorithm," vol. 17, pp. 434–450, March 1999.

[11] J. Barnes, A. Chi, L. Cutler, D. Healey, D. Leeson, T. McGunigal, J. Mullen, W. Smith, R. Sydnor, R. Vessot, and G. Winkler, "Characterization of frequency stability," *IEEE Transactions on Instrument Measurements*, 1971.

[12] F. L. Walls and D. W. Allan, "Measurements of frequency stability," in *Proceedings of the IEEE Special Issue*, vol. 74, pp. 162–168, IEEE, 1986.

[13] S. Loyka and A. Kouki, "On MIMO channel capacity, correlations, and keyholes: analysis of degenerate channels," *IEEE Transactions on communications*, vol. 50, pp. 1886–1888, December 2002.

[14] P. Almers, F. Tufvesson, and A. F. Molisch, "Measurement of keyhole effect in a wireless multiple-input multiple-output (MIMO) channel," *IEEE Communications Letters*, vol. 7, pp. 373–375, August 2003.

[15] S. Wyne, P. Almers, G. Ericsson, J. Karedal, F. Tufvesson, and A. F. Molisch, "Outdoor to indoor MIMO measurments at 5.2 ghz," in *Proc. VTC-Fall*, (Los Angeles, USA), pp. –, IEEE, 2004.